Dalton Transactions

Accepted Manuscript

ROYAL SOCIETY OF CHEMISTRY

www.rsc.org/dalton

Can aliphatic anchoring groups be utilised with dyes for p-type dye sensitized solar cells?

Yan Hao,[a†] Christopher J. Wood,[†b,c] Charlotte A. Clark,[b] James A. Calladine,[b] Raphael Horvath,[b] Magnus W. D. Hanson-Heine,[b] Xue-Zhong Sun,[b] Ian P. Clark,[e] Michael Towrie,[e] Michael W. George*,[b,d] Xichuan Yang,[a]* Licheng Sun,[a.f] Elizabeth A. Gibson*[b,c]

[a] *DUT-KTH Joint Research Centre on Molecular Devices, State Key Laboratory of Fine Chemicals, Dalian University of Technology (DUT), Dalian, China.*

[b] *School of Chemistry, The University of Nottingham, University Park, Nottingham, NG7 2RD, UK.*

[c] *Now at School of Chemistry, Newcastle University, Newcastle upon Tyne, NE1 7RU, United Kingdom.*

[d] *Department of Chemical and Environmental Engineering, University of Nottingham Ningbo China, 199 Talking East Road, Ningbo 315100, China.*

[e] *Central Laser Facility, Research Complex at Harwell, Science and Technology Facilities Council, Rutherford Appleton Laboratory, Harwell Campus, Didcot, Oxfordshire, OX11 0QX, United Kingdom*

[f] *KTH Royal Institute of Technology, Department of Chemistry, 10044 Stockholm, SE 10044, Sweden.*

Abstract

A series of novel laterally anchoring tetrahydroquinoline derivatives have been synthesized and investigated for their use in NiO-based p-type dye-sensitized solar cells. The kinetics of charge injection and recombination at the NiO-dye interface for these dyes have been

thoroughly investigated using picosecond transient absorption and time-resolved infrared measurements. It was revealed that despite the anchoring unit being electronically decoupled from the dye structure, charge injection occurred on a sub picosecond timescale. However, rapid recombination was also observed due to the close proximity of the electron acceptor on the dyes to the NiO surface, ultimately limiting the performance of the p-DSCs.

Introduction

The dye-sensitized solar cell (DSC) is a low cost alternative to crystalline silicon photovoltaics that converts sunlight into electricity using a dye adsorbed on a transparent, nanostructured semiconductor electrode, surrounded by a redox electrolyte. Almost all the current research in photocatalysis and dye-sensitized solar cells is focused on n-type systems, typically based on TiO_2.[1] Unlike the standard DSC, which has a passive counter electrode, tandem devices simultaneously use two photoelectrodes to harvest a greater proportion of the spectrum more efficiently.[2,3] Incorporation of a photocathode in tandem with a TiO_2-based n-type photoanode in a single device should give rise to a substantial increase in voltage and efficiency. By choosing sensitizers which absorb high energy photons on one electrode and low energy photons on the other, more of the solar spectrum can be utilised.[4] Tandem DSCs have not yet beaten the best n-type DSCs because the poor performance of dye-sensitized photocathodes limits the overall efficiency. Therefore it is necessary to improve the light conversion efficiency of dye-sensitized photocathodes in the long wavelength region of the solar spectrum so that they can match the best dye-sensitized photoanodes which typically collect and convert light between 400-700 nm.

Several groups have developed panchromatic organic sensitizers for TiO_2.[5–7] These generate high photocurrents (*ca.* 14 mA cm^{-2} for dyes TH304 and T4BTD-A in references 5 and 7),

however, the efficiencies are rarely higher than those obtained using dyes with a narrower absorption band. This is because shifting the absorption spectrum to longer wavelengths requires the frontier orbital separation of the dye to be reduced, bringing the HOMO and LUMO closer in energy. Lowering the energy of the LUMO lessens the driving force for electron injection into the TiO_2 conduction band. This can be offset by adding lithium ions to reduce the energy of the conduction band edge, however this also leads to a decrease in the photovoltage. The same effect is observed when the energy of the HOMO is increased, as this reduces the driving force for electron transfer to the oxidised dye from the redox mediator, thus increasing the rate of the competing recombination reactions between the electrons in the TiO_2 and holes in the dye. By using a tandem cell configuration, where the differences in energy between the redox couple and the valence and conduction band edges of the respective photocathode and anode are smaller at one electrode than the other, the low energy photons can be used to generate current without sacrificing the overall device voltage. To develop highly efficient tandem solar cells, the efficiency of the photocathode must be increased to match the conventional dye-sensitized TiO_2 solar cells.[8]

Recently, significant improvements to NiO-based p-DSCs have been made by designing dyes which promote charge separation and limit the recombination between the sensitizer and/or electrolyte and the semiconductor.[9–14] Currents obtained in these devices have reached over 8 mA cm^{-2} at 1 sun illumination.[4,15] Earlier, we reported a high performance dye based on a triphenyl amine electron donor and a cationic indolium acceptor unit that absorbed in this region.[4] The tandem DSCs incorporating this dye generated a photocurrent that was larger than any previously reported tandem DSC. However, it was notably lower than that of the single junction p-DSC. Inspection of the IPCE spectra of the individual n-DSC and p-DSCs

showed that there was still significant overlap between the two dyes used at opposite electrodes in the tandem DSC.

Here we describe a series of tetrahydroquinoline derivatives (Figure 1) which absorb up to 850-900 nm when adsorbed to mesoporous NiO via a lateral propionic acid chain. In the majority of donor-π-acceptor organic sensitizers reported, the anchoring group, typically carboxylic acid, is positioned close to an electron donating group. The electron donor is typically a modified triaryl amine, which fixes the excited state reduction potential ($E_{D^*/D}$-) to 1-1.4 V *vs*. NHE.[16,17] By separating the anchoring group from the electron donor, a wider choice of derivatives is possible and fine-tuning of the energy levels can be achieved. This could minimise energy wastage in the system and allow the shifting of the absorption towards the infrared. These new dyes are likely to inject charge (h^+) using a different mechanism to dyes that have been extensively studied in the past, dependent on their geometry on the semiconductor surface.

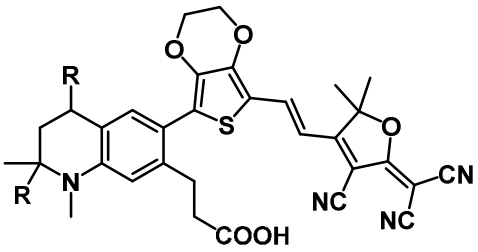

R= H, Dye 1
R= C_6H_{13}, Dye 2

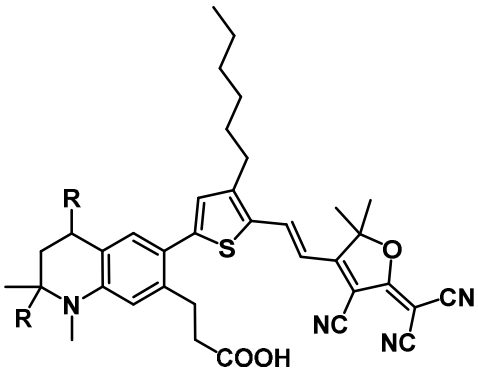

R= H, Dye 3
R= C_6H_{13}, Dye 4

Figure 1. The series of laterally anchored tetrahydroquinoline derivatives investigated here.

We have applied a combination of picosecond time-resolved transient absorption (TA) spectroscopy in the near-infrared and visible regions, together with time-resolved infrared (TRIR) spectroscopy to investigate the charge-transfer intermediates and fast injection/recombination dynamics of organic sensitizers adsorbed to NiO. The effect of the new anchoring group and different substituents around the dye on the charge transfer rates and device efficiency of p-DSCs incorporating the dyes have been compared. These measurements shed new light on the importance of dye-dye, dye-semiconductor and dye-electrolyte interactions to photoelectrochemical systems, such that modifications to the dye design can be made to improve the device efficiency.

Experimental Section

Solvents were dried by standard procedures. All other chemicals were purchased from commercial sources and used without further purification.

Analytical Measurements.

^{1}H NMR spectra were recorded with a Varian INOVA 400 NMR instrument. MS data were obtained with GCT CA156 (UK) high-resolution mass spectrometer (HRMS) or HP1100 LC/MSD (USA) mass spectrometer. UV-visible absorption spectra of the dyes in solutions were recorded in a quartz cell with 1 cm path length on a HP 8453 spectrophotometer. Electrochemical redox potentials were obtained by cyclic voltammetry and differential pulse voltammetry using a three-electrode cell and an IviumStat potentiostat. A solution of Bu_4NPF_6 (0.1 M) in CH_3CN was used as supporting electrolyte. The working electrode was a glassy carbon electrode, the auxiliary electrode was a Pt mesh, and the reference electrode was Ag^+/Ag in a solution of the supporting electrolyte. Ferrocene was used as an external calibrant. Samples for FTIR spectroscopy were prepared as either a KBr pressed disk (dye

only) or by adsorbing the dye on a mesoporous NiO film deposited on a CaF_2 window (Crystran). The NiO films were prepared by spraying a saturated solution of $NiCl_2$ in acetylacetone onto the surface of the CaF_2 window which was pre-heated to 450°C on a hotplate; this was then allowed to cool slowly to room temperature to give a compact film of NiO. The mesoporous layer was then deposited on top of the compact layer using an F108–templated precursor solution containing $NiCl_2$ (1 g), Pluronic® co-polymer F108 (1 g), Milli-Q water (3 g) and ethanol (6 g) and the excess was removed with a glass rod. The film was sintered at 450 °C for 30 minutes and an additional layer of precursor solution was applied and sintered to increase the film thickness. Infrared absorption spectra were recorded on a Thermo Nicolet 380 FTIR spectrometer for 16 scans at a resolution of 2 cm^{-1}.

Synthesis.

Compounds **3** and **4** were synthesized as previously reported.[18,19]

Ethyl-3-(6-bromo-1,2,2,4-tetramethyl-1,2,3,4-tetrahydroquinolin-7-yl)propanoate（5）

3 (3.87 g, 13.4 mmol) and N-Bromosuccinimide (NBS) (2.63 g, 14.7 mmol) were dissolved in 20 ml CCl_4. The mixture was stirred at room temperature for 2 h. The solvent was removed by rotary evaporation and the residue was purified by chromatography (silica gel, dichloromethane: hexane = 1:2) to provide **5** (yield 93 %). ^{1}H NMR (400 MHz, $CDCl_3$) δ 7.19 (s, 1H), 6.42 (s, 1H), 4.14 (q, *J* = 7.1 Hz, 2H), 2.97 (m, 2H), 2.80 (m, 4H), 2.62 (m, 2H), 1.75 (dd, *J* = 13.0, 4.5 Hz, 1H), 1.48 (t, *J* = 12.9 Hz, 1H), 1.27 (dt, *J* = 9.7, 6.9 Hz, 9H), 1.17 (s, 3H). GCT/TOF HRMS-EI (*m/z*): $[M]^+$ calcd for $C_{18}H_{26}NO_2$, 367.1147; found, 367.1154.

Ethyl-3-(6-bromo-2,4-dihexyl-1,2-dimethyl-1,2,3,4-tetrahydroquinolin-7-yl)propanoate（6）

The synthesis of compound **6** was conducted in a similar way to that of compound **5** (yield 78.9 %). ^{1}H NMR (400 MHz, $CDCl_3$) δ 7.20 (s, 1H), 6.42 (s, 1H), 4.14 (q, *J* = 7.1 Hz, 2H), 2.96 (m, 2H), 2.73 (s, 3H), 2.62 (dd, *J* = 8.7, 6.8 Hz, 3H), 1.66 (m, 2H), 1.37 (m, 23H), 1.14 (s, 3H), 0.89 (dt, *J* = 13.7, 6.8 Hz, 6H). GCT/TOF HRMS-EI (*m/z*): $[M]^+$ calcd for $C_{28}H_{46}NO_2$, 507.2712; found, 507.2721.

Ethyl-3-(6-(2,3-dihydrothieno[3,4-b][1,4]dioxin-5-yl)-1,2,2,4-tetramethyl-1,2,3,4-tetrahydroquinolin-7-yl)propanoate (7)

$Pd(PPh_3)_4$ (60 mg, 0.05 mmol), **5** (770.7 mg, 2.1 mmol) and **1** (1.33 g, 3.1 mmol) were dissolved in dry Toluene (20 ml). The mixture was refluxed overnight. The reaction system was cooled to room temperature, the solvent was removed by rotary evaporation and the residue was purified by chromatography (silica gel, dichloromethane: Petroleum ether = 1:2) to provide **7** (yield 63 %). API-ES MS (Positive, m/z): calcd. for $C_{24}H_{31}NO_4S$, 429; found, 429.

Ethyl-3-(6-(2,3-dihydrothieno[3,4-b][1,4]dioxin-5-yl)-2,4-dihexyl-1,2-dimethyl-1,2,3,4-tetrahydroquinolin-7-yl)propanoate (8)

The synthesis of compound **8** was conducted in a similar way to that of compound **7** (yield 69 %). API-ES MS (Positive, m/z): calcd. for $C_{34}H_{51}NO_4S$, 569; found, 569.

Ethyl-3-(6-(4-hexylthiophen-2-yl)-1,2,2,4-tetramethyl-1,2,3,4-tetrahydroquinolin-7-yl)propanoate (9)

$Pd(PPh_3)_2Cl_2$ (35 mg, 0.05 mmol), **5** (770.7 mg, 2.1 mmol) and **2** (1.42 g, 3.1 mmol) were dissolved in dry THF (20 ml). The mixture was refluxed overnight. The reaction system was

cooled down to room temperature, the solvent removed by rotary evaporation and the residue was purified by chromatography (silica gel, dichloromethane: hexane = 1:2) to provide **9** (yield 62 %). API-ES MS (Positive, m/z): calcd. for $C_{28}H_{41}NO_2S$, 455; found, 455.

Ethyl-3-(2,4-dihexyl-6-(4-hexylthiophen-2-yl)-1,2-dimethyl-1,2,3,4-tetrahydroquinolin-7-yl)propanoate (10)

The synthesis of compound **10** was conducted in a similar way to that of compound **9** (yield 45 %). API-ES MS (Positive, m/z): calcd. for $C_{38}H_{61}NO_2S$, 595; found, 595.

Ethyl-3-(6-(7-formyl-2,3-dihydrothieno[3,4-b][1,4]dioxin-5-yl)-1,2,2,4-tetramethyl-1,2,3,4-tetrahydroquinolin-7-yl)propanoate (11), ethyl-3-(6-(7-formyl-2,3-dihydrothieno[3,4-b][1,4]dioxin-5-yl)-2,4-dihexyl-1,2-dimethyl-1,2,3,4-tetrahydroquinolin-7-yl)propanoate (12), ethyl-3-(6-(5-formyl-4-hexylthiophen-2-yl)-1,2,2,4-tetramethyl-1,2,3,4-tetrahydroquinolin-7-yl)propanoate (13), ethyl 3-(6-(5-formyl-4-hexylthiophen-2-yl)-2,4-dihexyl-1,2-dimethyl-1,2,3,4-tetrahydroquinolin-7-yl)propanoate (14)

$POCl_3$ (0.24 ml, 2.6 mmol) was added dropwise with stirring to a solution of **7, 8, 9 or 10** (2.5 mmol) and DMF (0.2 ml, 2.6 mmol) in dichloromethane at 0 ºC. The mixture was then held under reflux overnight and then cooled, ice (30 g) was added, and NaOH solution (5 %) added until a pH of 6 was obtained. The mixture was extracted further with dichloromethane (3 × 20 ml) and water, the combined organic layers were dried over $MgSO_4$. The solvent was removed by rotary evaporation and the residue as the crude products of **11**, **12**, **13** or **14** were used for next step without further purification.

Ethyl-(E)-3-(6-(7-(2-(4-cyano-5-(dicyanomethylene)-2,2-dimethyl-2,5-dihydrofuran-3-yl)vinyl)-2,3-dihydrothieno[3,4-b][1,4]dioxin-5-yl)-1,2,2,4-tetramethyl-1,2,3,4-tetrahydroquinolin-7-yl)propanoate (15)

A mixture of **11** (0.14 mmol), 2-dicyanomethylen-3-cyano-4,5,5-trimethyl-2,5-dihydrofuran (28 mg, 0.14 mmol), pyridine (5 ml), and several drops of acetic acid as a catalyst was stirred at room temperature for 12 h. Pyridine was removed by distilling under reduced pressure. The resulting coarse product was extracted further with dichloromethane (3 × 20 ml) and water. Then the residue was purified by chromatography (silica gel, dichloromethane) to provide **15** (dark solid, yield 44 %). GCT/TOF HRMS-EI (*m/z*): calcd for $C_{36}H_{38}N_4O_5S$, 638.2563; found, 638.2565.

Ethyl-(E)-3-(6-(7-(2-(4-cyano-5-(dicyanomethylene)-2,2-dimethyl-2,5-dihydrofuran-3-yl)vinyl)-2,3-dihydrothieno[3,4-b][1,4]dioxin-5-yl)-2,4-dihexyl-1,2-dimethyl-1,2,3,4-tetrahydroquinolin-7-yl)propanoate (16)

The synthesis of compound **16** was conducted in a similar way to that of compound **15** (yield 73 %). GCT/TOF HRMS-EI (*m/z*): calcd for $C_{46}H_{58}N_4O_5S$, 778.4128; found, 778.4132.

Ethyl-(E)-3-(6-(5-(2-(4-cyano-5-(dicyanomethylene)-2,2-dimethyl-2,5-dihydrofuran-3-yl)vinyl)-4-hexylthiophen-2-yl)-1,2,2,4-tetramethyl-1,2,3,4-tetrahydroquinolin-7-yl)propanoate (17)

The synthesis of compound **17** was conducted in a similar way to that of compound **15** (yield 57 %). API-ES MS (Positive, m/z): calcd. for $C_{40}H_{48}N_4O_3S$, 664; found, 664.

Ethyl-(E)-3-(6-(5-(2-(4-cyano-5-(dicyanomethylene)-2,2-dimethyl-2,5-dihydrofuran-3-yl)vinyl)-4-hexylthiophen-2-yl)-2,4-dihexyl-1,2-dimethyl-1,2,3,4-tetrahydroquinolin-7-yl)propanoate (18)

The synthesis of compound **18** was conducted in a similar way to that of compound **15** (yield 60 %). GCT/TOF HRMS-EI (*m/z*): calcd for $C_{50}H_{68}N_4O_3S$, 804.5012; found, 804.5026.

(E)-3-(6-(7-(2-(4-cyano-5-(dicyanomethylene)-2,2-dimethyl-2,5-dihydrofuran-3-yl)vinyl)-2,3-dihydrothieno[3,4-b][1,4]dioxin-5-yl)-1,2,2,4-tetramethyl-1,2,3,4-tetrahydroquinolin-7-yl)propanoic acid (Dye 1)

15 (0.41 mmol), dry ethanol (6.2 ml) and 2 M LiOH aqueous solution (4.0 ml, 4.0 mmol) were mixed in a 10 ml flask and then stirred overnight. The reaction mixture was diluted by water and pH adjusted to 6 by adding 1 M HCl. The mixture was diluted with 100 ml of 1 M citric acid and washed with ethyl acetate (3 × 75 ml). The combined organic layers were washed with ice-cold H_2O (3 × 100 ml), dried ($MgSO_4$), and concentrated under reduced pressure. After chromatography purification (silica gel, CH_2Cl_2 : MeOH = 30 : 1 as eluent), the target compounds were obtained as dark solids (yield 43 %).^{1}H NMR (400 MHz, Acetone) δ 10.50 (s, 1H), 8.06 (d, *J* = 15.7 Hz, 1H), 7.08 (s, 1H), 6.85 (d, *J* = 15.7 Hz, 1H), 6.61 (s, 1H), 4.54 (dd, *J* = 5.0, 3.1 Hz, 2H), 4.40 (dd, *J* = 5.2, 3.0 Hz, 2H), 2.97 (m, 2H), 2.91 (s, 3H), 2.84 (d, *J* = 17.4 Hz, 1H), 2.54 (m, 2H), 1.84 (m, 7H), 1.48 (t, *J* = 12.9 Hz, 1H), 1.33 (m, 6H), 1.24 (s, 3H). API-ES MS (Negative, m/z): calcd. for $C_{34}H_{34}N_4O_5S$, 610; found, 610.

(E)-3-(6-(7-(2-(4-cyano-5-(dicyanomethylene)-2,2-dimethyl-2,5-dihydrofuran-3-yl)vinyl)-2,3-dihydrothieno[3,4-b][1,4]dioxin-5-yl)-2,4-dihexyl-1,2-dimethyl-1,2,3,4-tetrahydroquinolin-7-yl)propanoic acid (Dye 2)

The synthesis of compound **Dye 2** was conducted in a similar way to that of **Dye 1** (yield 77 %). ^{1}H NMR (400 MHz, Acetone) δ 8.05 (d, *J* = 15.7 Hz, 1H), 7.11 (s, 1H), 6.84 (d, *J* = 15.7 Hz, 1H), 6.63 (s, 1H), 4.54 (dd, *J* = 5.1, 3.0 Hz, 2H), 4.39 (dd, *J* = 5.1, 3.0 Hz, 2H), 2.97 (m, 2H), 2.88 (d, *J* = 4.7 Hz, 3H), 2.71 (d, *J* = 9.0 Hz, 2H), 2.54 (m, 2H), 1.82 (m, 7H), 1.48 (m, 21H), 1.24 (s, 3H), 0.89 (q, *J* = 6.8 Hz, 7H).

(E)-3-(6-(5-(2-(4-cyano-5-(dicyanomethylene)-2,2-dimethyl-2,5-dihydrofuran-3-yl)vinyl)-4-hexylthiophen-2-yl)-1,2,2,4-tetramethyl-1,2,3,4-tetrahydroquinolin-7-yl)propanoic acid (Dye 3)

The synthesis of **Dye 3** was conducted in a similar way to that of compound **Dye 1** (yield 47 %). ^{1}H NMR (400 MHz, Acetone) δ 8.36 (d, *J* = 15.6 Hz, 1H), 7.24 (s, 1H), 7.21 (s, 1H), 6.75 (d, *J* = 15.5 Hz, 1H), 6.64 (s, 1H), 3.12 (d, *J* = 8.3 Hz, 2H), 2.93 (s, 3H), 2.89 (m, 3H), 2.60 (m, 2H), 1.85 (d, *J* = 5.9 Hz, 7H), 1.71 (m, 2H), 1.50 (t, *J* = 12.9 Hz, 1H), 1.33 (m, 12H), 1.25 (s, 3H), 0.88 (t, *J* = 7.0 Hz, 3H).

(E)-3-(6-(7-(2-(4-cyano-5-(dicyanomethylene)-2,2-dimethyl-2,5-dihydrofuran-3-yl)vinyl)-2,3-dihydrothieno[3,4-b][1,4]dioxin-5-yl)-2,4-dihexyl-1,2-dimethyl-1,2,3,4-tetrahydroquinolin-7-yl)propanoic acid (Dye 4)

The synthesis of compound **Dye 4** was conducted in a similar way to that of compound **Dye 1** (yield 65 %). ^{1}H NMR (400 MHz, Acetone) δ 8.57 (d, *J* = 15.5 Hz, 1H), 7.49 (s, 1H), 7.43 (s, 1H), 6.97 (d, *J* = 15.6 Hz, 1H), 6.89 (s, 1H), 3.36 (d, *J* = 3.7 Hz, 2H), 3.12 (m, 5H), 2.95 (m, 1H), 2.83 (m, 2H), 2.07 (d, *J* = 8.7 Hz, 7H), 1.94 (m, 2H), 1.82 (m, 4H), 1.57 (m, 23H), 1.48 (s, 3H), 1.12 (dt, *J* = 13.5, 6.9 Hz, 9H).

Density Functional Theory Calculations.

Frequency calculations were performed for **Dye 1** using the Q-Chem software package.[20] The neutral **Dye 1** molecule and its corresponding mono-anion were evaluated using the restricted and unrestricted B3LYP methods, with the 6-311G(d,p) basis set. Initial geometries were optimised at the same level of theory, to minimum energy structures in order to allow for harmonic vibrational analysis, which was performed using analytical second derivatives of

the energy with respect to nuclear displacement. The resulting frequencies have been scaled by 0.9682.[21]

Ultrafast Transient Absorption and Time-Resolved Infrared Spectroscopy.

Ultrafast TRIR spectra in CH_2Cl_2 solution were collected using the Nottingham ultrafast TRIR apparatus described in detail previously.[22,23] Briefly, this comprises of a Ti:sapphire oscillator (Spectra Physics, MaiTai) and regenerative amplifier system (Spectra Physics, Spitfire Pro) to generate 800 nm laser pulses (fwhm = 150 fs) at a frequency of 1 kHz. This output is split into two parts, the first of which pumps a TP-1 harmonic generator to generate pump pulses (650 nm). The second part is used to pump a TOPAS-C-OPA with a frequency generator unit to generate tuneable IR probe pulses (fwhm = 150 fs) with a spectral bandwidth of *ca*. 180 cm^{-1} and pulse energy of *ca*. 2 μJ (both at 2000 cm^{-1}). A delay between the pump and probe beams, ranging from 0.5 ps up to 2 ns, is achieved using an optical delay line (Aerotech), before the pump beam is focused onto the sample using a quartz lens. The IR pulses generated are split by a Germanium beam splitter into a reference and probe beam. The reference beam is detected by a separate single element Mercury-Cadmium-Telluride (MCT) detector (Kolmar Technology). At the sample the overlap of the pump and probe is such that the pump beam is slightly larger in diameter (*ca*. 400 μm) than that of the probe (*ca*. 200 μm). After passing through the sample the probe is split into its component frequencies by a 250 mm IR monochromator (Spectral Products, DK240) containing either 150 or 300 grooves/mm diffraction gratings (giving spectral resolutions of either 4 or 2 cm^{-1} respectively). The intensities of these component frequencies are measured by a 128 element MCT array detector (Infrared Associates) and both these signals and that of the single

element detector are amplified by a 144-channel amplifier and digitized by a 16-bit analogue-to-digital converter (Infrared Systems Development Corp).

Samples for TRIR and TA spectroscopic measurements of the dyes on NiO were prepared as described above. The ULTRA laser system used for TRIR and TA spectroscopies on these samples has been described in detail elsewhere.[22,24] Briefly, a cryogenically cooled Ti:Sapphire laser amplifier (Thales Laser ALPHA 10000) provides 800 nm pulses with a duration of 50 fs at 10 kHz. The output is split to provide pump and probe beams. Computer controlled OPAs (Light Conversion) are used to generate both the 650 nm pump beam as well as a tuneable mid-IR probe used for experiments presented here. A portion of the beam is also used for white light continuum generation. The pump and probe beams are focussed to overlap at the sample with diameters of 100 and 50 μm respectively. After this the probe beam is dispersed onto two linear 128 element MCT detector arrays acquiring spectra at 10 kHz. Difference spectra are generated by modulating the pump laser output at 5 kHz using a chopper and energy/spectral instabilities of the laser are accounted for by taking a portion of the probe and dispersing it onto a second MCT detector array and used as a reference. The sample was mounted on a rapidly moving "XY raster" to prevent heating and photochemical decomposition.

Solar Cells

p-DSCs were made by depositing the precursor solution described above onto conducting glass substrates (Pilkington TEC15, sheet resistance 15 Ω/square) by the doctor-blade technique using Scotch tape as a spacer (0.2 cm^2 active area), followed by sintering in an oven at 450 °C for 30 min. The NiO electrodes were soaked in a CH_3CN solution of the dye (0.3 mM) for 16 h at room temperature. The dyed NiO electrode was assembled face-to-face

with a platinized counter electrode (Pilkington TEC8, sheet resistance 8 Ω/square) using a 30 mm thick thermoplastic frame (Surlyn 1702). The electrolyte, containing LiI (1.0 M) and I_2 (0.1 M) in CH_3CN, was introduced through the pre-drilled hole in the counter electrode, which was sealed afterwards. The UV-visible absorption spectra of the dyes adsorbed on NiO films were recorded using an Ocean Optics USB2000+VIS-NIR fibre-optic spectrophotometer. Current-voltage measurements were measured using an Ivium CompactStat potentiostat under AM 1.5 simulated sunlight from an Oriel 150 W solar simulator, calibrated with a Si photodioide, giving light with an intensity of 100 mW cm^{-2}. Incident photon-to-current conversion efficiencies were recorded by passing the light from the solar simulator through an Oriel Cornerstone 130 1/8m monochromator and recording the current from the solar cell with an Ivium CompactStat potentiostat which was calibrated against a Si photodiode.

Results

Dye synthesis

The synthesis of **Dyes 1-4** were conducted in eleven steps with moderate yields. Related synthetic procedures of these dyes are described in **Scheme 1**. The electron-donating tetrahydroquinolines **3** or **4** were obtained from 3-nitrocinnamic acid in 5 steps according to the previously reported procedures.[18,19] Compounds **3** and **4** were then reacted with N-Bromosuccinimide (NBS) to yield compounds **5** and **6**, respectively. The linkers were synthesised by reacting 3,4-Ethylenedioxythiophene (EDOT) or 3-hexylthiophene with $SnBu_3Cl$ to get rough intermediates **1** or **2** without purification. Using the classical Stille reaction, the compounds **7**, **8**, **9** and **10** were formed by connecting **5** and **6** with **1** or **2** using either catalytic procedure **c** or **d**. **Dyes 1-4** were obtained by formylation of compounds **7, 8,**

9 or **10** followed by Knoevenagel condensation reactions with 2-dicyanomethylen-3-cyano-4,5,5-trimethyl-2,5-dihydrofuran and finally hydrolysis of the propyl ester.

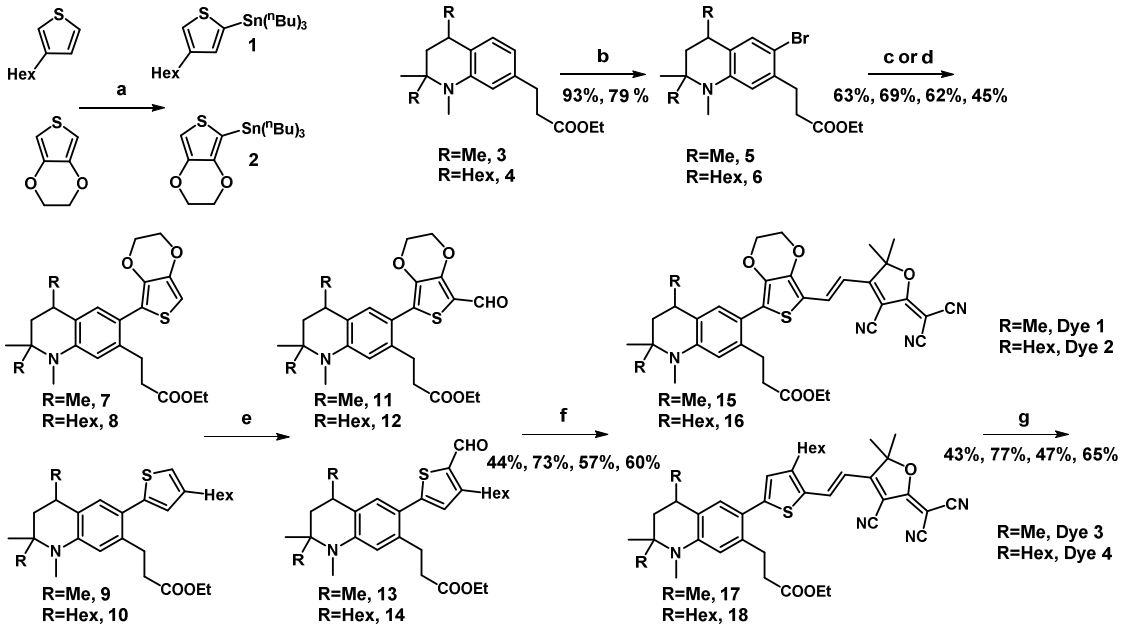

Scheme 1. Synthetic route for **Dye 1**, **Dye 2**, **Dye 3** and **Dye 4**. Reagents and conditions: (a) THF, ^{n}BuLi, $Sn(Bu)_3Cl$, -78°C to room temperature (r.t), 8 h; (b) CCl_4, NBS, 2 h, r.t, 93 %; (c) Toluene $Pd(PPh_3)_4$, reflux, overnight, 47 %; (d) THF, $Pd(PPh_3)_2Cl_2$, reflux, overnight, 53 %; (e) CH_2Cl_2, DMF/$POCl_3$, reflux, overnight; (f) 2-dicyanomethylen-3-cyano-4,5,5-trimethyl-2,5-dihydrofuran, pyridine, acetic acid, room temperature 12 h; (g) 2.0 M aqueous LiOH, EtOH, room temperature, overnight, quantitative.

Optical and Electrochemical Characterization.

The UV-visible absorption spectra of **Dyes 1-4** in CH_2Cl_2 solution and adsorbed on NiO films are shown in Figure 2 and the results are summarised in Table 1. Differential pulse voltammograms of **Dyes 2 & 4** are given in Figure S3 in the ESI.

Table 1: Optical and electrochemical properties of the **Dyes 1-4.**

Dye	Absorption			Emission	$E_{0\text{-}0}$ [c]	$E_{(D/D-)}$ [e]	$E_{(D^*/D-)}$ [e]
	λ_{max} [a]	ε at λ_{max}	λ_{max} D|NiO	λ_{max} [a]	(eV)	(V vs. $Fe(Cp)_2^{+/0}$)	

	(nm)	(L mol^{-1} cm^{-1})	(nm)[b]	(nm)			
Dye 1	601	29 960	613	794	1.72	-1.07	0.66
Dye 2	603	35 840	618	789	1.74	-1.07	0.68
Dye 3	626	38 760	640	798	1.68	-1.02	0.67
Dye 4	634	35 940	649	800	1.67	-1.01	0.66

[a]Absorption and emission spectra were measured in CH_2Cl_2 solution (2×10^{-5} M) at room temperature. [b]Absorption spectra on NiO were obtained through measuring the dye adsorbed on a NiO film from an CH_3CN dye solution. [d] The zero−zero singlet excited-state level (E_{0-0}) was calculated with the wavelength at the intersection (λ_{inter}) of the emission and absorption spectra with the equation E_{0-0} (eV) = 1240/λ_{inter} (nm). [d]The reduction potential of the dyes were measured in CH_3CN with 0.1 M Bu_4NPF_6 as electrolyte (working electrode: glassy carbon; reference electrode: Ag/Ag^+; calibrated with $FeCp_2^{+/0}$ as an external standard, counter electrode: Pt). [e]$E_{(D^*/D^-)}$ was estimated to be the reduction potential of the dye plus E_{0-0}.

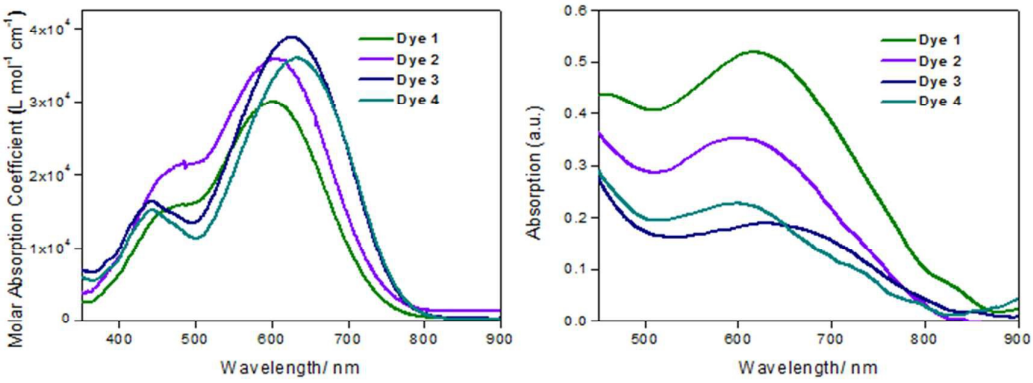

Figure 2. UV-visible absorption spectra of the dyes **Dye 1** (green), **Dye 2** (violet), **Dye 3** (blue) and **Dye 4** (cyan) in CH_2Cl_2 (left) and adsorbed on NiO (right).

All the dyes exhibit one prominent band in the absorption spectra in solution, appearing at *ca.* 600 nm with a shoulder at *ca.* 450 nm, which are both attributed to π-π* transitions. These values are similar to that observed for the previously reported dye **HY103**, which has the same donor and acceptor moieties as the dyes in this study.[19,25] The strong electron withdrawing nature of the (3-cyano-4,5,5-trimethyl-2(5H)-furanylidene)maleonitrile acceptor unit appears to red-shift the absorption maximum for these dyes compared to dyes reported previously which incorporate a tetrahydroquinoline electron donor and a cyanoacrylic acid

acceptor (e.g. λ_{max} = 440 nm for the dye **C2-1**).[18,26–28] A bathochromic shift of the maximum absorption from 600 nm for **Dyes 1 & 2** with ethylenedioxothiophene spacers to *ca.* 630 nm for **Dyes 3 & 4** dyes with hexylthiophene spacers was observed.

$E_{0\text{-}0}$ energies in the range of 1.67-1.74 eV were extracted from the intersection of the normalized absorption and emission spectra, for **Dyes 1-4**. The driving force for charge injection (ΔG_{inj}) from the dye to the NiO and for regeneration (ΔG_{reg}) of the dye by the electrolyte was estimated (Table S2 in the ESI) from the ground and excited state reduction potentials ($E'_{(D/D\text{-})}$ and $E'_{(D^*/D\text{-})}$) of the dyes in solution and the approximate potential of the valence band edge of NiO and the redox potential of the electrolyte ($E'(I_3^-/I^-)$.[†29] $E'_{(D^*/D\text{-})}$ for each dye is more positive than the valence band edge of NiO. ΔG_{inj} for these dyes was in the range between 0.77–0.80 eV, which is slightly lower than that which is usually reported for organic sensitizers on NiO (typically ΔG_{inj} > 1 eV); this means less energy is wasted in the injection step. Previously, He *et al.* proposed that a minimum of ΔG_{inj} = *ca.* 0.8 eV is required for charge injection to occur efficiently, suggesting that charge injection is favourable for these dyes on NiO. ΔG_{reg} for these dyes is in the range between 0.19–0.25 eV, which suggests that dye regeneration by I_3^-/I^- is less favourable.

There have been a number of reports on how the π-linker can modify the redox properties of a D-π-A dye in solution.[30–33] The hexyl thiophene linkers in **Dye 3** and **Dye 4** positively shift the reduction potential and subsequently decrease ΔG_{reg} compared to the ethylenedioxythiophene linker in **Dyes 1** and **2** ($E_{(D/D\text{-})}$ for **Dye 4** is *ca.* 50 mV more positive than $E_{(D/D\text{-})}$ for **Dye 2**). This is consistent with previous observations for p-type triphenylamine dyes (e.g. **O7**, EDOT linker, $E_{(D/D\text{-})}$ = -0.84 *vs.* NHE; **O2**, thiophene linker, $E_{(D/D\text{-})}$ = –0.78 *vs.* NHE).[30]

Adsorption of the dyes onto NiO (D|NiO) resulted in a broadening and bathochromic shift of the absorption band for all the dyes (*ca.* 15 nm). For example, Figure S1 in the ESI compares the overlaid spectra for **Dye 1** in solution and on NiO. This is usually attributed to the coupling of the dye with the semiconductor surface when conjugated anchoring groups are used. However, in the dyes presented here, the anchoring group is electronically decoupled from the dye so the shift in the electronic spectra must be attributed to the association of the bulk dye with the metal oxide surface. To investigate the association of the dyes with the NiO surface we measured the FTIR absorption spectra of the dyes alone (in a KBr pressed disc) and adsorbed on NiO (deposited on CaF_2 windows). Both spectra are shown for **Dye 1** and **Dye 1|NiO** in Figure 3 and comparisons of the key peaks are given in Table S1 in the ESI. It is clear that the peak corresponding to the C=O stretch at 1751 cm^{-1} present in the KBr spectrum was absent in the spectrum of the dye adsorbed onto NiO.[34,35] This is strong evidence for the dye anchoring through the carboxylic acid.[36] The peak at 2227 cm^{-1} corresponding to the C≡N stretch does not shift when the dye is adsorbed onto NiO.[37] However, the shoulder at 2209 cm^{-1} observed in the KBr spectrum was absent when the dye was immobilised on NiO. It is possible that this the result of a secondary binding mode to NiO *via* maleonitrile group on the acceptor unit. Alternatively the shoulder could arise from hydrogen bonding between dye molecules in the solid state which is disrupted when the dye is immobilised on NiO. An expanded view of these peaks are given in Figure S2 in the ESI.

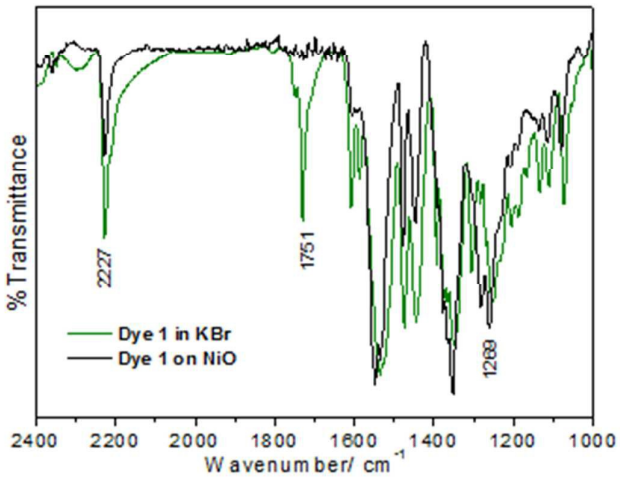

Figure 3. FTIR spectra of **Dye 1** in a KBr disk (green) and **Dye 1|NiO** (black).

The peaks at 1251 and 1269 cm^{-1} which correspond to the C–N stretches in the tetrahydroquinlone and the peaks at 1525 and 1537 cm^{-1} which correspond to aromatic C=C stretches in the KBr spectrum are shifted by *ca.* + 10 cm^{-1} in the NiO spectrum. One explanation for this behaviour is that the dye lies flat on the NiO surface. However, this may not be indicative of how the dye would orientate in a p-DSC in the presence of a liquid redox mediator such as LiI/LiI_3 in CH_3CN.

Solution TRIR Measurements

To examine the photophysical behaviour of **Dye 1** in CH_2Cl_2 solution we have used TRIR in both the ν(CN), organic ν(CO) and fingerprint regions. *ps*-TRIR spectra recorded in all regions following 650 nm excitation are shown (at selected delays) in Figure 4 below.

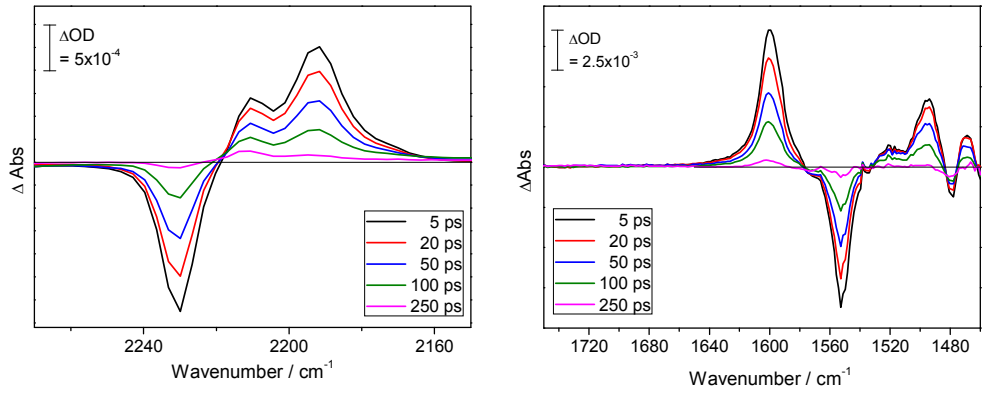

Figure 4. ps-TRIR spectra of **Dye 1** in CH_2Cl_2 after excitation with a 650 nm laser pulse at selected time delays in the ν(CN) (left) and organic ν(CO) and fingerprint regions (right).

In the ν(CN) region immediately following photolysis the parent band at 2228 cm^{-1} is bleached and new bands are apparent at 2210 and 2193 cm^{-1}. The observed red-shift is consistent with an increase in electron density on the CN ligands, consistent with a "push-pull" dye.[4,17] In the organic ν(CO) and fingerprint regions, following photolysis parent bleaches are observed at 1554 and 1479 cm^{-1} and new bands at 1600, 1519, 1495 and 1470 cm^{-1}. We observe no signal for the carboxylic acid anchoring group consistent with our hypothesis that the electron density on the anchor is not affected by the electronic transition. All the transient bands decay to reform the parent, with a lifetime of *ca.* 70 (± 15) ps (Figure S5 in the ESI).

Ultrafast Transient Absorption Measurements

Ultrafast transient absorption measurements were undertaken of the dyes adsorbed onto NiO in both the visible and near-IR regions (500-1100 nm). The spectra recorded are shown in Figure 5.

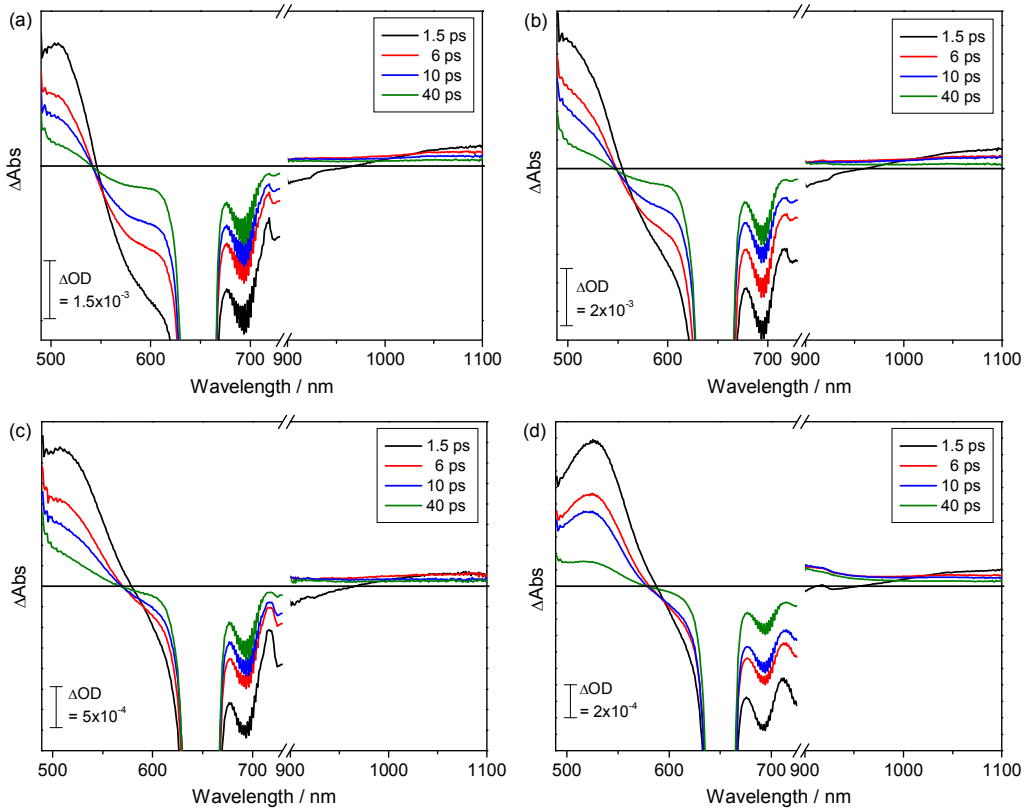

Figure 5. ps-Vis-NIR transient absorption spectra of the dyes adsorbed on NiO at selected time-delays after excitation with a 650 nm laser pulse: (a) **Dye 1**|NiO , (b) **Dye 2**|NiO, (c) **Dye 3**|NiO and (d) **Dye 4**|NiO.

All of the dyes exhibited similar spectra following irradiation at 650 nm with excitation resulting in bleaching of the absorption bands and formation of transient bands located at *ca.* 500 nm (Table 2) assigned as the anionic dyes. Additionally, a broad feature is observed in the near-IR region of the spectra similar to that reported previously attributed to the oxidation of the NiO.[16,38–40] The decay of both species for each dye were determined by fitting bi-exponentials and the fitted lifetimes are shown in Table 2. The lifetimes for all four dyes on NiO were < 30 ps and as such it might be expected that the dye regeneration step in a p-DSC device will not be able to compete with recombination. This will limit the photocurrent generated by p-DSCs incorporating these devices *vide infra*. In order to investigate the *push-*

pull mechanism further we have undertaken TRIR measurements which allows more structural insight.

Table 2. Band positions (from TA) and determined lifetimes for the radical anion (from TA and TRIR) of **Dye 1**|NiO **, Dye 2**|NiO, **Dye 3**|NiO and **Dye 4**|NiO excited at 650 nm **(**obtained by fitting a bi-exponential function to the kinetic traces)**.**

		Lifetime (τ) / ps			
	Anion band λ_{max} / nm	**TA**		**TRIR**	
Dye 1	507	1.6 (± 0.2)	14 (± 1)	2.1 (± 0.5)	24 (± 3)
Dye 2	494	2 (± 0.2)	17 (± 2)	2.3 (± 0.4)	27 (± 5)
Dye 3	509	3.5 (± 0.5)	28 (± 7)	2.2 (± 0.9)	25 (± 4)
Dye 4	526	3.5 (± 0.6)	24 (± 6)	1.2 (± 0.2)	20 (± 2)

Ultrafast TRIR measurements

The ground state FTIR spectrum of **Dye 1**|NiO provided in Figure 3 contains bands at 1353, 1447, 1477, 1544 and 1605 cm^{-1}. Figure 6 shows the TRIR spectra of **Dye 1**|NiO at different delay times after excitation at 650 nm. The TRIR spectrum of the film 1 ps following photolysis (650 nm) shows that the parent bands are bleached and new features are produced at 1320, 1414, 1475, 1508, and 1585 cm^{-1}. As illustrated in Figure 6b, these bands are not stable and decay to reform the parent with time-constants of 2.1 ps and 24 ps. From our experiments, we were unable to resolve the rate of initial charge separation to form the reduced dye radical anions, which appears to take place on a sub-picosecond timescale.[14] Ultrafast charge separation is well documented for metal-free sensitizers on NiO when carboxylic acid anchoring groups conjugated to the chromophore are used.

Scaled harmonic frequency calculations were carried out for **Dye 1** at the B3LYP/6-311G(d,p) level on both the neutral and mono-anionic forms. The band positions resulting from these calculations provide a good match with the TRIR spectra in Figure 6(a), and offer additional support for the assignment of the experimental spectra as depletion of the neutral species, followed by formation of the anionic state. A complete list of the associated frequencies and intensities can be found in Table S4 in the ESI.

These experiments suggest that charge separation between the dye and NiO can take place despite the electronic decoupling of the anchor. This is consistent with a previous reports that demonstrate sub-picosecond charge-separation from NiO with simple ruthenium and iridium complexes with electronically decoupled methyl phosphonic acid anchors, and perylenes which bind through benzoic acid.[17,41,42] However, we were surprised to find such rapid electron transfer for flexible, aliphatic anchoring groups in this study.

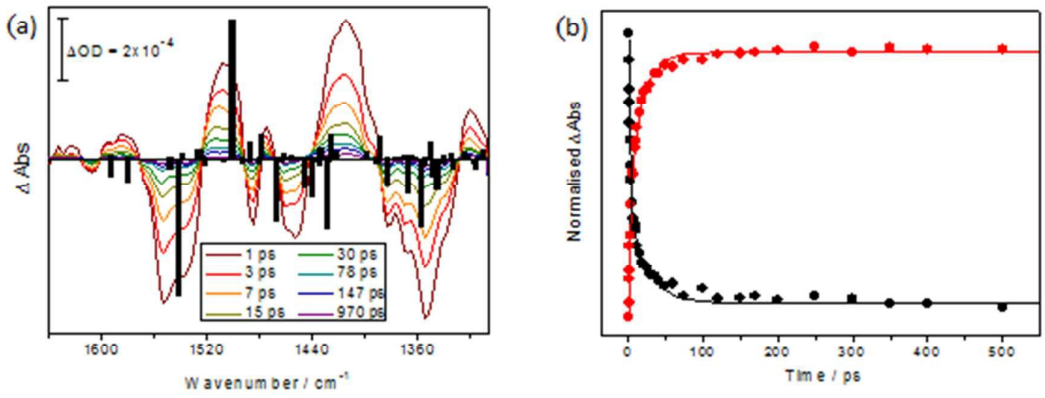

Figure 6. ps-TRIR spectra of **Dye 1**|NiO observed after excitation with a 650 nm laser pulse. (a) ps-TRIR spectra at a number of time-delays with the corresponding theoretical band positions shown as black bars. The calculated neutral bands have been set negative for visual clarity. The oscillator strengths have been normalised. (b) Biexponential decay of the band at 1414 cm^{-1} (black dots) and simultaneous reformation of the parent band at 1353 cm^{-1} (red dots).

We also investigated **Dye 2**|NiO, **Dye 3**|NiO and **Dye 4**|NiO using TRIR (Figure S4 in the ESI). Comparing the dyes recorded adsorbed on NiO versus those recorded for **Dye 1** in solution, there are differences in band positions and lifetimes. From this we propose that an excited state for these dyes is formed following photolysis in solution and on NiO we are observing charge-separation (with rapid recombination). Additionally, on NiO the transient bands for the related structures (**Dye 1**|NiO and **Dye 2**|NiO) and (**Dye 3**|NiO and **Dye 4**|NiO) are at similar positions (Table S3 in the ESI). The shifts in frequency from the ground to photoexcited state are indicative of increased electron density upon the thiophene and maleonitrile groups.

The decay of the transient signals occurs within 1 ns for all the dyes examined. Again, this is in spite of the non-conjugated anchoring group, suggesting that the dyes are in close proximity to the NiO surface. Similar rates of charge recombination to those in this study are seen with the simple squaraine dye **SQ** in reference 14 (10-200 ps). It was concluded that this was a result of small spatial separation between the electron density on the anionic dye and the hole in the NiO. The lifetimes of the charge separated state between $NiO^{+}|D^{-}$ are shown in Table 2 and there is close agreement with the values obtained using TA and TRIR. Therefore we have shown that TRIR is a valuable tool for examining the nature of the radical anion formed on illumination of a dye-sensitized photocathode. The technique avoids large regions of the transient spectrum being obscured by filters and the pump laser. Additionally, it is particularly useful for dyes such as those examined here that give broad signals in the NIR region, which overlap with signals from the charge carriers in the metal oxide and give little structural information regarding the transient intermediate formed.

p-Type Dye-Sensitized Solar Cells.

The photovoltaic performance of p-DSCs based on these sensitized by **Dye**s **1-4** is summarized in Table 3. Photocurrent density-voltage curves, dark current curves and IPCE spectra are given in Figures S6-9 the ESI.

Table 3. Photovoltaic Performance of DSCs Based on **Dye 1, Dye 2**, **Dye 3** and **Dye 4.**

Dye	J_{SC}[a] **(mA cm^{-2})**	V_{OC}[b] **(mV)**	***FF*[c] (%)**	η[d] **(%)**
Dye 1	0.97	45	31	0.017
Dye 2	1.22	70	35	0.030
Dye 3	0.93	55	34	0.017

Dye 4	0.89	72	37	0.024
[e]**NiO**	0.21	56	41	0.005

[a]J_{SC} is the short-circuit current density at the $V = 0$ intercept, [b]V_{OC} is the open-circuit voltage at the $J = 0$ intercept, [c]FF is the device fill factor, [d]η is the power conversion efficiency, [e] device constructed using an undyed NiO film.

Under standard AM 1.5G sunlight irradiation (100 mW cm^{-2}), the overall conversion efficiency of the **Dye 2**-sensitized solar cell is the highest. The V_{OC} obtained for these devices were lower than those typically obtained for p-DSCs (90-120 mV) and the trends in V_{OC} followed the trends in the onset of the dark currents. All four dyes in this study generated relatively low photocurrents, similar to a number of previously reported dyes which absorb at longer wavelengths.[43,44] However, upon inspection of the IPCE spectra for these dyes (Figure S8 in the ESI) it is clear that there was little or no contribution to the photocurrent as a result of absorption of light by the dyes at their absorption maxima. Evidence from the FTIR spectrum of **Dye 1** on NiO indicates there is an interaction between the acceptor part of the dye and the NiO. This suggests that this dye lies in close proximity to the NiO surface, in the absence of the liquid redox mediator. This could explain the rapid charge recombination, despite the anchoring group being electronically decoupled from the dye. We attribute the very low photocurrents to the short lifetimes (10-30 ps) of the charge separated states observed, which suggests that charge recombination occurs before the dye can transfer an electron to the redox couple.

The IPCE at 400 nm for the p-DSCs in this study were in the region of 20-25%. I_3^-/I^- solutions are strongly coloured with an absorption maximum at 360 nm. The photocurrent response seen at λ <450 nm could be result of charge injection by the diiodide radical following the photolysis of I_3^-.[29,44–46] However, the photocurrent generated by a dye-free NiO

device (0.2 mA cm^{-2}) was lower than those obtained with the dyed p-DSCs. The UV-visible absorption spectra of the dyes in Figure 2 contain a second, higher energy absorption band at *ca.* 450 nm. Zhu *et al.* previously reported that energy transfer from the excited dye to I_3^- can result in charge injection by the $I_2^{\bullet-}$ radical.[45] IPCE spectra of **Dye 2** and undyed NiO taken from 330-550 nm are given in Figure S9 in the ESI, from this it is apparent that light absorption by the dye does not contribute to the photocurrent in these devices. In agreement with reference 48, there is a slight enhancement to the photocurrent at the wavelengths attributed to injection by $I_2^{\bullet-}$ radical when the dye is present. One possible explanation for this is that the dye interacts with the electrolyte and increases the local concentration of I_3^- close to the NiO surface.[47–49] However we note that there can be significant variation in the photocurrent generated in the absence of a dye due to slight differences in the film thickness (±50 nm) and exposed NiO surface.

Conclusions

Photoinduced charge-separation between the series of laterally anchored dyes and NiO occurred on an ultrafast timescale (τ_{inj} < 1 ps). This is despite the anchoring group being electronically decoupled from the surface. The driving force for charge-separation is slightly lower than is usually found for organic sensitizers on NiO and, therefore, less energy is wasted in the injection step and more light is collected at longer wavelengths. This supports our efforts to shift the absorption maxima of the dyes to lower energy as required for tandem DSCs. However, results from the IPCE measurements indicate that very little photocurrent is being generated at the absorption maxima of these dyes. The ultrafast TA and TRIR experiments revealed that rapid recombination between the photoreduced dye and the h^+ at the NiO surface competes with regeneration of the dye by I_3^- in the electrolyte. Evidence from the FTIR and UV-visible absorption spectroscopies is suggestive of electronic interaction between the dye and the NiO, suggesting the dye lies in close proximity to the

NiO surface. This close proximity is a likely cause of the rapid recombination. TRIR has been used to investigate charge separation between NiO and a sensitizer. For these experiments, the charge-transfer mechanism appears to be straight forward – we appear to form one photo-induced product from one ground state. However we envisage that this tool will be increasingly important for more complex systems with more additional intermediate states or in the presence of additional species such as in our work to investigate photocatalysis using dye-sensitized NiO.

Acknowledgements

EAG gratefully acknowledges the Royal Society for Funding a Dorothy Hodgkin Research Fellowship, a 2nd Year Research Grant and an International Joint Project with Dalian University of Technology. CJW thanks the EPSRC and The University of Nottingham for a DTA studentship.

Footnotes

† E_{VB}(NiO) ≈ 0.5 V vs. NHE in 100 mM $LiClO_4$ in CH_3CN, estimated using spectroelectrochemistry in reference 32. $E°'(I_3^-/I_2^{\bullet-})$ in CH_3CN ≈ −0.2 V vs. NHE, also in reference 32.

References

1 A. Hagfeldt, G. Boschloo, L. Sun, L. Kloo and H. Pettersson, *Chem. Rev.*, 2010, **110**, 6595–6663.

2 A. Nattestad, M. Ferguson, R. Kerr, Y.-B. Cheng and U. Bach, *Nanotechnology*, 2008, **19**, 295304–295313.

3 J. He, H. Lindström, A. Hagfeldt and S.-E. Lindquist, *Sol. Energy Mater. Sol. Cells*, 2000, **62**, 265–273.

4 C. J. Wood, G. H. Summers and E. A. Gibson, *Chem. Commun.*, 2015, **51**, 3915–3918.

5 H. N. Tian, X. C. Yang, R. K. Chen, A. Hagfeldt and L. C. Sun, *Energ. Environ. Sci.*, 2009, **2**, 674–677.

6 S. Kolemen, O. A. Bozdemir, Y. Cakmak, G. Barin, S. Erten-Ela, M. Marszalek, J.-H. Yum, S. M. Zakeeruddin, M. K. Nazeeruddin, M. Graetzel and E. U. Akkaya, *Chem. Sci.*, 2011, **2**, 949–954.

7 R. Stalder, D. Xie, A. Islam, L. Han, J. R. Reynolds and K. S. Schanze, *Appl. Mater. Inter*, 2014, **6**, 8715–8722.

8 F. Odobel and Y. Pellegrin, *J. Phys. Chem. Lett.*, 2013, **4**, 2551–2564.

9 K. A. Click, D. R. Beauchamp, B. R. Garrett, Z. Huang, C. M. Hadad and Y. Wu, *Phys. Chem. Chem. Phys.*, 2014, **16**, 26103–26111.

10 Z. Liu, W. Li, S. Topa, X. Xu, X. Zeng, Z. Zhao, M. Wang, W. Chen, F. Wang, Y.-B. Cheng and H. He, *Appl. Mater. Inter*, 2014, **6**, 10614–10622.

11 S. Powar, Q. Wu, M. Weidelener, A. Nattestad, Z. Hu, A. Mishra, P. Bäuerle, L. Spiccia, Y.-B. Cheng and U. Bach, *Energ. Environ. Sci.*, 2012, **5**, 8896–8900.

12 J. C. Freys, J. M. Gardner, L. D'Amario, A. M. Brown and L. Hammarström, *Dalt. Trans.*, 2012, **41**, 13105–13111.

13 L. Le Pleux, A. L. Smeigh, E. Gibson, Y. Pellegrin, E. Blart, G. Boschloo, A. Hagfeldt, L. Hammarström and F. Odobel, *Energ. Environ. Sci.*, 2011, **4**, 2075–2084.

14 J. Warnan, J. Gardner, L. Le Pleux, J. Petersson, Y. Pellegrin, E. Blart, L. Hammarström and F. Odobel, *J. Phys. Chem. C*, 2014, **118**, 103–113.

15 Q.-Q. Zhang, K.-J. Jiang, J.-H. Huang, C.-W. Zhao, L.-P. Zhang, X.-P. Cui, M.-J. Su, L.-M. Yang, Y.-L. Song and X.-Q. Zhou, *J. Mater. Chem. A*, 2015, **3**, 7695–7698.

16 C. J. Wood, M. Cheng, C. A. Clark, R. Horvath, I. P. Clark, M. L. Hamilton, M. Towrie, M. W. George, L. Sun, X. Yang and E. A. Gibson, *J. Phys. Chem. C*, 2014, **118**, 16536–16546.

17 P. Qin, J. Wiberg, E. A. Gibson, M. Linder, L. Li, T. Brinck, A. Hagfeldt, B. Albinsson and L. Sun, *J. Phys. Chem. C*, 2010, **114**, 4738–4748.

18 R. Chen, X. Yang, H. Tian, X. Wang, A. Hagfeldt and L. Sun, *Chem. Mater.*, 2007, **19**, 4007–4015.

19 Y. Hao, X. Yang, J. Cong, H. Tian, A. Hagfeldt and L. Sun, *Chem. Commun.*, 2009, 4031–4033.

20 Y. Shao, L. F. Molnar, Y. Jung, J. Kussmann, C. Ochsenfeld, S. T. Brown, A. T. B. Gilbert, L. V. Slipchenko, S. V. Levchenko, D. P. O'Neill, R. a DiStasio, R. C.

Lochan, T. Wang, G. J. O. Beran, N. A. Besley, J. M. Herbert, C. Y. Lin, T. Van Voorhis, S. H. Chien, A. Sodt, R. P. Steele, V. A. Rassolov, P. E. Maslen, P. P. Korambath, R. D. Adamson, B. Austin, J. Baker, E. F. C. Byrd, H. Dachsel, R. J. Doerksen, A. Dreuw, B. D. Dunietz, A. D. Dutoi, T. R. Furlani, S. R. Gwaltney, A. Heyden, S. Hirata, C.-P. Hsu, G. Kedziora, R. Z. Khalliulin, P. Klunzinger, A. M. Lee, M. S. Lee, W. Liang, I. Lotan, N. Nair, B. Peters, E. I. Proynov, P. A. Pieniazek, Y. M. Rhee, J. Ritchie, E. Rosta, C. D. Sherrill, A. C. Simmonett, J. E. Subotnik, H. L. Woodcock, W. Zhang, A. T. Bell, A. K. Chakraborty, D. M. Chipman, F. J. Keil, A. Warshel, W. J. Hehre, H. F. Schaefer, J. Kong, A. I. Krylov, P. M. W. Gill and M. Head-Gordon, *Phys. Chem. Chem. Phys.*, 2006, **8**, 3172–3191.

21 J. P. Merrick, D. Moran and L. Radom, *J. Phys. Chem. A*, 2007, **111**, 11683–11700.

22 M. Towrie, D. C. Grills, J. Dyer, J. A. Weinstein, P. Matousek, R. Barton, P. D. Bailey, N. Subramaniam, W. M. Kwok, C. Ma, D. Phillips, A. W. Parker and M. W. George, *Appl. Spec.*, 2003, **57**, 367–380.

23 J. A. Calladine, R. Horvath, A. J. Davies, A. Wriglesworth, X. Z. Sun and M. W. George, *Appl. Spec.*, 2015, **69**, 519–524.

24 G. M. Greetham, P. Burgos, C. Qian, I. P. Clark, P. S. Codd, R. C. Farrow, M. W. George, M. Kogimtzis, P. Matousek, A. W. Parker, M. R. Pollard, D. A. Robinson, X. Zhi-Jun and M. Towrie, *Appl. Spec.*, 2010, **64**, 1311–1319.

25 M. Ziółek, J. Karolczak, M. Zalas, Y. Hao, H. Tian and A. Douhal, *J. Phys. Chem. C*, 2014, **118**, 194–205.

26 R. Chen, X. Yang, H. Tian and L. Sun, *J. Photochem. Photobiol. A*, 2007, **189**, 295–300.

27 C.-R. Zhang, L. Liu, J.-W. Zhe, N.-Z. Jin, Y. Ma, L.-H. Yuan, M.-L. Zhang, Y.-Z. Wu, Z.-J. Liu and H.-S. Chen, *Int. J. Mol. Sci.*, 2013, **14**, 5461–5481.

28 Y. Hao, X. Yang, J. Cong, A. Hagfeldt and L. Sun, *Tetrahedron*, 2012, **68**, 552–558.

29 E. A. Gibson, L. Le Pleux, J. Fortage, Y. Pellegrin, E. Blart, F. Odobel, A. Hagfeldt and G. Boschloo, *Langmuir*, 2012, **28**, 6485–6493.

30 Z. Ji, G. Natu, Z. Huang and Y. Wu, *Energ. Environ. Sci.*, 2011, **4**, 2818–2821.

31 W.-H. Liu, I.-C. Wu, C.-H. Lai, C.-H. Lai, P.-T. Chou, Y.-T. Li, C.-L. Chen, Y.-Y. Hsu and Y. Chi, *Chem. Commun.*, 2008, 5152–5154.

32 H. Ellis, S. K. Eriksson, S. M. Feldt, E. Gabrielsson, P. W. Lohse, R. Lindblad, L. Sun, H. Rensmo, G. Boschloo and A. Hagfeldt, *J. Phys. Chem. C*, 2013, **117**, 21029–21036.

33 Z. Liu, D. Xiong, X. Xu, Q. Arooj, H. Wang, L. Yin, W. Li, H. Wu, Z. Zhao, W. Chen, M. Wang, F. Wang, Y. B. Cheng and H. He, *Appl. Mater. Inter*, 2014, **6**, 3448–3454.

34 Y. Hao, X. Yang, J. Cong, X. Jiang, A. Hagfeldt and L. Sun, *RSC Adv.*, 2012, **2**, 6011–6017.

35 F. Zhang, F. Shi, W. Ma, F. Gao, Y. Jiao, H. Li, J. Wang, X. Shan, X. Lu and S. Meng, *J. Phys. Chem. C*, 2013, **117**, 14659–14666.

36 J. Y. Park, B. Y. Jang, C. H. Lee, H. J. Yun and J. H. Kim, *RSC Adv.*, 2014, **4**, 61248–61255.

37 S. Jiang, S. Fan, X. Lu, G. Zhou and Z.-S. Wang, *J. Mater. Chem. A*, 2014, **2**, 17153–17164.

38 G. Boschloo and A. Hagfeldt, *J. Phys. Chem. B*, 2001, **105**, 3039–3044.

39 J.-F. Lefebvre, X.-Z. Sun, J. A. Calladine, M. W. George and E. A. Gibson, *Chem. Commun.*, 2014, **50**, 5258–5260.

40 A. Morandeira, G. Boschloo, A. Hagfeldt and L. Hammarström, *J. Phys. Chem. B*, 2005, **109**, 19403–19410.

41 Y. Pellegrin, L. Le Pleux, E. Blart, A. Renaud, B. Chavillon, N. Szuwarski, M. Boujtita, L. Cario, S. Jobic, D. Jacquemin and F. Odobel, *J. Photochem. Photobiol. A*, 2011, **219**, 235–242.

42 M. Gennari, F. Légalité, L. Zhang, Y. Pellegrin, E. Blart, J. Fortage, A. M. Brown, A. Deronzier, M. N. Collomb, M. Boujtita, D. Jacquemin, L. Hammarström and F. Odobel, *J. Phys. Chem. Lett.*, 2014, **5**, 2254–2258.

43 C. H. Chang, Y. C. Chen, C. Y. Hsu, H. H. Chou and J. T. Lin, *Org. Lett.*, 2012, **14**, 4726–4729.

44 D. Ameline, S. Diring, Y. Farre, Y. Pellegrin, G. Naponiello, E. Blart, B. Charrier, D. Dini, D. Jacquemin and F. Odobel, *RSC Adv.*, 2015, **5**, 85530–85539.

45 H. Zhu, A. Hagfeldt and G. Boschloo, *J. Phys. Chem. C*, 2007, **111**, 17455–17458.

46 G. Boschloo and A. Hagfeldt, *Acc. Chem. Res.*, 2009, **42**, 1819–1826.

47 J. B. Asbury, Y.-Q. Wang, E. Hao, H. N. Ghosh and T. Lian, *Res. Chem. Intermed.*, 2001, **27**, 393–406.

48 X. Li, A. Reynal, P. Barnes, R. Humphry-Baker, S. M. Zakeeruddin, F. De Angelis and B. C. O'Regan, *Phys. Chem. Chem. Phys.*, 2012, **14**, 15421–15428.

49 M. Pastore, E. Mosconi and F. De Angelis, *J. Phys. Chem. C*, 2012, **116**, 5965–5973.

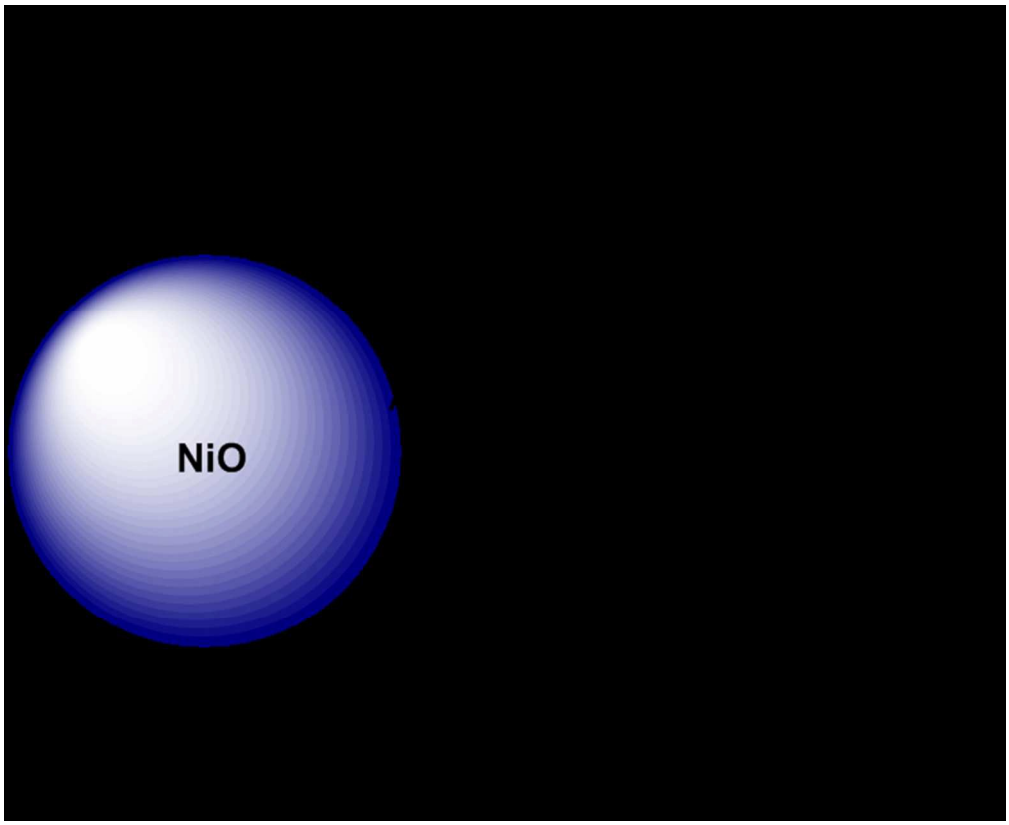

123x101mm (150 x 150 DPI)